Optimization of the Crystallization Process of TFA-MOD ErBCO Films on IBAD-Substrate Under Low-Pressure Conditions via DSD Approach

W. Freitag, M. Erbe, J. Hänisch, and B. Holzapfel

***Abstract*—Crystallization in a sub-atmospheric reactor could achieve higher production rate while dramatically reducing the flow rate of high-purity carrier gas. Due to enhanced supersaturation conditions at low total pressure, it is necessary to find the optimum processing window to avoid misoriented growth. This is extensive and incomplete when using one-factor-at-a-time experiments as significant parameters are often correlated. We prepared $ErBa_2Cu_3O_{7-\delta}$ (ErBCO) films by the TFA-MOD route with low-fluorine solutions on technical IBAD template with CeO_2 top buffer layer in an industrial reel-to-reel furnace. We used a novel design-of-experiment (DOE) technique, the Definitive Screening Design (DSD), to identify significant factors for improving critical temperature and microstructure of the films. Within the investigated range, lower crystallization temperature as well as lower total pressure are beneficial. With the new process window, the self-field critical current density at 77 K was successfully increased from almost zero to 1 MA/cm^2. This shows that DSD is an attractive approach to optimize the CSD process under low-pressure conditions to enhance the growth rate or possibly achieve a reduction of carrier gas flow rate by a factor $p_{\mathrm{tot}}/p_{\mathrm{atm}}$ of 3.3 for equal output as the atmospheric reactor. Further improvement of J_c is necessary and possible.**

***Index Terms*—Chemical solution deposition CSD, definitive screening design DSD, design of experiments DOE, REBCO film.**

I. Introduction

FOR ideal gases, the gas diffusion constant D depends on the total pressure p as $D \propto 1/p_{\mathrm{tot}}$. Therefore, crystallization in a sub-atmospheric reactor could dramatically enhance the film growth rate and yield higher production rate. It also allows realizing the same throughput as the atmospheric reactor, but with a carrier gas flow rate lower by a factor of $p_{\mathrm{tot}}/p_{\mathrm{atm}}$ and therefore a much lower consumption of high-purity gas. However, this acceleration of nucleation leads to more undesired a-axis and randomly oriented grains due to enhanced supersaturation conditions at low total pressure. Consequently, it is necessary to find the optimum processing window to maximize c-axis nucleation. This includes specific process parameters such as temperature, oxygen partial pressure, water partial pressure, and gas flow, but also variables that are hard to control, such as substrate surface energy and precursor permeability [1].

There are just a few studies reported for processing *RE*BCO films at sub-atmospheric pressure by the TFA-MOD route, all on YBCO, and the results have not been transferred to metallic tapes yet [2], [3]. Furthermore, the optimization was often performed using one-factor-at-a-time (OFAT) experiments, where only one parameter is changed at a time while all others are kept constant. This type of optimization is time-consuming and often incomplete since essential parameters that influence and determine the final film quality are often interrelated. On the one hand, the OFAT approach often does not find these interactions, on the other hand, many experiments are necessary to optimize the process conditions. Another currently investigated research method for fast screening a plentitude of samples is high-throughput experimentation (HTE), which has recently already been used for the optimization of a large number of parameters in the field of superconductivity [4].

In this work, we prepared $ErBa_2Cu_3O_{7-\delta}$ (ErBCO) films by the TFA-MOD route with low-fluorine solutions on technical IBAD templates with CeO_2 top buffer layer. In order to investigate these preparation method in conditions as close as possible to the complex industrial environment, the pyrolysis was performed reel-to-reel in a 6 m long industrial furnace with 18 heating zones. ErBCO is one of the *RE*BCO compounds with potential as a superconducting layer for coated conductors due to its achievable high critical current densities, J_c, in a wide window of the crystallization temperature compared to other *RE* elements [5]. This is favorable for large-scale production in a reel-to-reel process.

For these experiments, we introduced a certain design-of-experiment (DOE) technique, namely Definitive Screening Design (DSD) [6]. This allowed the identification of significant factors, their interactions and quadratic effects in order to improve the superconducting properties while minimizing the number of necessary experiments. Previous results already demonstrated the benefits of DSD for improving ErBCO on short tape samples at ambient pressure [7] as well as $BaZrO_3$-YBCO nanocomposite films [8]. Here, we also varied the total pressure, which has a tremendous influence on the whole process with significant implications for the parameter space. However, since DSD requires finite target values for each sample, we considered J^{sf}(77 K)

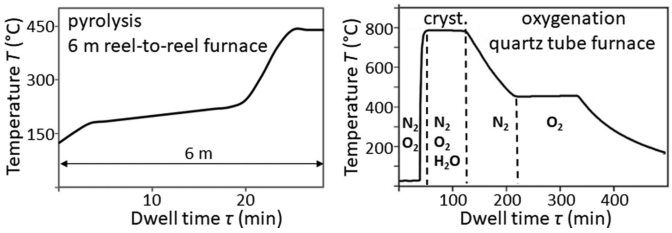

Fig. 1. Treatment of pyrolysis (left) and crystallization/oxygenation (right).

as unfavourable. Instead, we started the parameter optimization with respect to the critical temperature T_c and the full width at half maximum (FWHM) of the (005) ErBCO rocking curve as a measure for the degree of out-of-plane orientation. We used this as a criterion for the structural quality with reference to the epitaxial growth of the films. The results were compared to SEM images. As a next step, we increased J_c^{sf}(77 K).

II. Experimental

A. Solution and Sample Preparation

For preparing the low-fluorine solution, fluorinated and non-fluorinated precursor salts Er-propionate, Ba-TFA and Cu-propionate were mixed in the stoichiometric ratio Er:Ba:Cu = 1:2:3 in a mixture of 90 vol.-% methanol and equal amounts of the iso-alcohols ethanol to tetradecane resulting in a concentration of 0.25 M yttrium. Additional ethyl cellulose was added to increase the viscosity. 12 mm wide SuperOx IBAD tape with a layer architecture of CeO_2 on $MgO/Y_2O_3/Al_2O_3$/Hastelloy C276 was used as substrate. The solution was deposited by slot-die coating over a length of 2 m in a continuous reel-to-reel process at 12 m/h inside a chamber with a constant dew point of 16 °C in pure nitrogen, and subsequently pyrolyzed in an 18-zone tube furnace with 6 m length and 60 mm inner diameter. The gas (30% O_2 in N_2) had a dew point of 19 °C and a speed of 14.3 cm·s^{-1}. The profile of the heat treatment is shown in Fig. 1. Short samples of 1 cm × 1 cm cut out of the pyrolyzed tape were used for the combined crystallization and oxygenation steps in a quartz tube with gas supply inside a tubular three-zone furnace. The investigated factors were crystallization temperature (T_{crys}), oxygen partial pressure (p_{O2}), total pressure (p_{tot}), dwell time (τ_{crys}), flow of nitrogen (F_{N2}), and water partial pressure (p_{H2O}), which was set by the flow of water (F_{H2O}). The oxygenation followed for all samples in dry O_2 with a gas speed of 3.4 cm·s^{-1} at 450 °C for about two hours with subsequent furnace cooling to 200 °C (Fig. 1).

B. Definitive Screening Design (DSD) and Data Analysis

In DSD, the main effects are independent of two-factor interactions and those are not confounded. It is therefore possible to estimate non-confounded main and quadratic effects with a minimal number of experiments and maximal precision. DSD requires 3 levels (low, center, and high) for each factor to detect and identify any factor causing a strong nonlinear effect. Table I shows the levels of the factors for the first DSD (A) run.

TABLE I
Investigated Factors X_i and Their Levels for the First DSD (A) Run

Level (coded units)	X_1 T_{crys} (°C)	X_2 p_{O2} (mbar)	X_3 p_{tot} (mbar)	X_4 τ_{crys} (min)	X_5 F_{N2} (L/min)	X_6 F_{H2O} (g/h)
Min (-1)	770	0.15	250	45	2	1.5
Center (0)	780	0.225	500	60	3	3
Max (1)	790	0.3	750	75	4	4.5

TABLE II
Design Matrix With Coded Units for the First DSD (A) Run Corresponding to Table I

Sample №	x_1 T_{crys}	x_2 p_{O2}	x_3 p_{tot}	x_4 τ_{crys}	x_5 F_{N2}	x_6 F_{H2O}
A1	0	1	1	1	1	1
A2	0	-1	-1	-1	-1	-1
A3	1	0	-1	1	1	-1
A4	-1	0	1	-1	-1	1
A5	1	-1	0	-1	1	1
A6	-1	1	0	1	-1	-1
A7	1	1	-1	0	-1	1
A8	-1	-1	1	0	1	-1
A9	1	1	1	-1	0	-1
A10	-1	-1	-1	1	0	1
A11	1	-1	1	1	-1	0
A12	-1	1	-1	-1	1	0
A13 c.r.	0	0	0	0	0	0
A14 c.r.	0	0	0	0	0	0

Additional center run (grey) to estimate the population variance regardless of significant factors.

We used the statistical software package JMP for this approach. Table II shows the design matrix for the investigated factors, which is generated by using a so-called conference matrix [9]. Coded units (−1, 0, 1) correspond to the levels in Table I. The minimum number of trials is $2m + 1$ (m: number of factors). The design was built around six factors, which implies that 13 experiments are required. But the trial with level 0 of all factors, the center run (c.r.), was repeated, see bottom of Table II, which is necessary for estimating the population variance regardless of the significant factors and to verify the reproducibility [10].

The relationship between the value to be optimized, also denoted as response y_i, and the process parameters x_i is expected to be nonlinear involving second order interaction effects:

$$y_i = \beta_0 + \sum \beta_j x_{ij} + \sum \beta_{ik} x_i x_k + \sum \beta_{ji} x_i^2 + \varepsilon_i \quad (1)$$

where the parameters $\beta_0, \ldots, \beta_{ii}$ are unknown constants that are associated with all possible main effects x_n, 2-factor interactions $x_i x_k$, and quadratic effects x_i^2; and ε_i is the scatter range of the normal distribution. Of a variety of reasonable models, the second-order model containing main, interaction and quadratic effects with minimum Bayesian information criterion (BIC) with finite correction was selected. BIC is an estimator to select a "good" model that can explain the predicted values well, while avoiding overfitting. Assuming the errors to follow independent and identical standard distributions, BIC is expressed via the

least square estimation in (2) [9].

$$\mathrm{BIC}\ (P) = n \ln\left(\hat{\sigma}^2\right) + |P| \ln(n) \tag{2}$$

where P is the number of parameters included in the model, n is the number of observations, and $\hat{\sigma}^2 = \Sigma(y_i - \widehat{y}_i)/n$ is the estimator of the variance of errors ε_i, where y_i and $\widehat{y}_i$ are observed and fitted value of the ith factor, respectively.

Based on the H_0 hypothesis, the significance of each effect is tested. It is assumed that a given effect is actually not significant. The significance of the effect is assessed based on its p-value, which describes the probability of falsely rejecting the H_0 hypothesis. It is defined by the tail probability in the standard t-distribution curve and computed by integrating the standard t-distribution function from t to infinite. An effect is significant, if $p \leq 0.05$ [11].

C. Characterization

We defined two normalized responses for the measured values of T_c and FWHM to be optimized by DSD first. The structural characteristics of the films were investigated by X-ray diffraction (XRD; SmartLab, Rigaku, Cu-$K_{\alpha 1}$) and scanning electron microscopy (SEM; LEO 1530, FEG by Zeiss). The superconducting properties were measured by inductive techniques, i.e., the self-field critical current density $J_{c,ind}^{sf}$(77 K) (Cryoscan, THEVA; 50 µV criterion) and the critical temperature T_c. Some of the best samples were investigated by electrical transport measurements, i.e., $J_c(B, 77\ \mathrm{K})$, in four-probe configuration in a physical properties measurement system (PPMS, Quantum Design; 1 $\mu V \cdot cm^{-1}$ criterion) with fields up to 9 T. Prior to that, the samples were photolithographically masked and structured by wet-chemical etching to achieve bridges of 50 µm width and 1 mm length. After a focused ion beam (FIB) cut (Helios NanoLab 600, FEI, in-lense detector, 3 kV), those bridges were further used for SEM analysis of the cross section and layer thickness.

D. Determination of the Responses for DSD

For all samples, the net induced voltage U_{ind} is normalized to its maximum value ($U_{ind,max} = 1$), hereafter referred to as U_{norm}. $T_{c,10}$, $T_{c,50}$ and $T_{c,90}$ are defined as the temperatures at which U_{norm} reaches 10, 50 and 90% of the value in the normal state. Furthermore, we normalized T_c in order to account for both an induced voltage $U_{ind,0} > 0$ at the start of the measurement (around 30 K) being indicative of an incomplete superconducting transition and for the transition width ($\Delta T_c = T_{c,90} - T_{c,10}$) as a measure of sample homogeneity. With that, samples with small transition widths and low $U_{ind,0}$ are rewarded while large values of both terms are penalized, as expressed in (3).

$$T_{c,norm} = T_{c,50} \times T_{c,50}/(T_{c,50} + \Delta T_c) \times (1 - U_{ind,0}) \tag{3}$$

For the rocking curve (rc) of the (005) ErBCO reflection, the (200) CeO_2 peak of the buffer was used as an internal standard. Every sample was aligned to this peak before the rocking curve was measured with a tilt of $\omega = \pm 10°$ around the longitudinal axis. We normalized the rocking curves to reward on the one hand a large fraction of c-axis grown ErBCO by a greater area A_{RC} and on the other hand a sharp texture by a small FWHM as shown in equation to (4).

$$A_{rc,norm} = A_{rc}\ /FWHM_{rc} \tag{4}$$

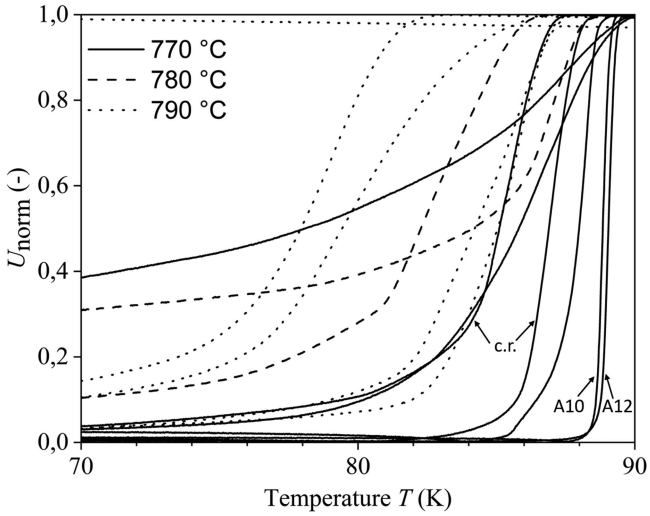

Fig. 2. Results of the inductive T_c measurement for first DSD (A) run.

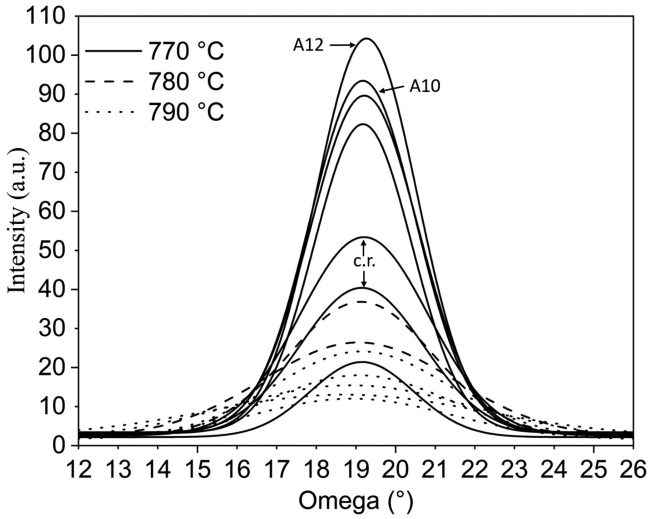

Fig. 3. Results of the rocking curve measurement for first DSD (A) run.

III. Results and Discussion

A. Inductive T_c and Rocking Curve

The values of the two center runs (c.r.) in the first DSD (A) run (thickness 760 nm ± 50 nm) vary within an acceptable range for both, T_c and rocking curve, Figs. 2 and 3 respectively. Two general trends emerge for T_{crys} and total pressure p_{tot}. The samples with the best or second best results for $T_{c,norm}$ and $A_{rc,norm}$ are No. A10 and No. A12. Both were crystallized at the lowest temperature of 770 °C and the lowest pressure of 250 mbar (Table II), whereas all samples without any T_c or low values for $T_{c,norm}$ and $A_{rc,norm}$ were crystallized at 780 °C or 790 °C.

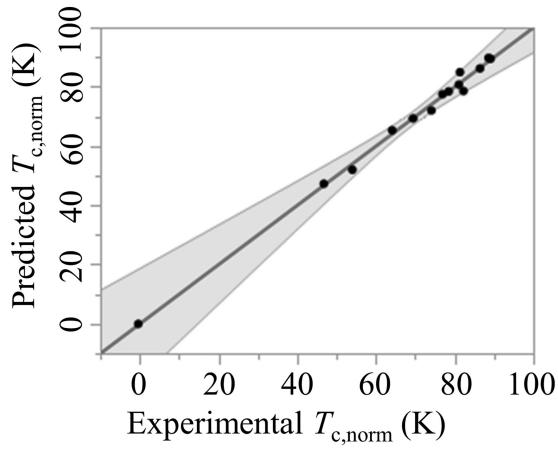

Fig. 4. Residual plot for $T_{c,norm}$ with predicted versus experimental values.

TABLE III
MODEL COEFFICIENTS OF THE SIGNIFICANT MAIN, INTERACTION AND QUADRATIC EFFECTS FOR $T_{C,NORM}$ WITH THEIR STANDARD ERRORS ε AND P-VALUES

Factor	Coefficient	Standard error ε	p - value
Intercept	81.77		
F_{H2O}	14.34	0.981	0.00013
p_{tot}	− 11.5	0.981	0.00030
T_{crys}	− 9.82	0.981	0.00056
$T_{crys} \times p_{O2}$	− 11.4	1.141	0.00056
τ_{crys}	8.14	0.981	0.00115
$(p_{O2})^2$	− 17.29	1.416	0.00135
$T_{crys} \times F_{H2O}$	8.29	1.217	0.00286

B. Definitive Screening Design Model Evaluation

The corresponding residual plot for $T_{c,norm}$ (5) is shown in Fig. 4 and has an R^2 of 0.99. The gray area depicts the mean linear deviation of the measured values from the predicted values. The significant effects are listed in Table III, each with its coefficient, standard error, and p-value.

$$\begin{aligned} T_{c,norm} = {} & 81.77 - 9.82 \times (T_{crys} - 780)/10 - 0.94 \\ & \times (p_{O2} - 225)/75 \\ & - 11.5 \times (p_{tot} - 500)/250 + 8.14 \times (\tau_{crys} - 60)/15 \\ & + 14.34 \times (F_{H2O} - 3)/1.5 \\ & - 11.4 \times (T_{crys} - 780)/10 \times (p_{O2} - 225)/75 \\ & + 8.29 \times (T_{crys} - 780)/10 \times (F_{H2O} - 3)/1.5 \\ & + 17.29 \times ((p_{O2} - 225)/75)^2 \end{aligned} \quad (5)$$

As expected from Fig. 2, this model means that lower T_{crys} and p_{tot} is beneficial for T_c. There is a quadratic effect of p_{O2}, and F_{N2} is not significant and set to 3 L/min for further investigations. There are also two-factor interactions of T_{crys} with p_{O2} and F_{H2O}. Furthermore, the model proposes that the maximum of T_c can be obtained with $T_{crys} = 770$ °C, $p_{O2} = 0.25$ mbar, $p_{tot} = 250$ mbar, $\tau_{crys} = 75$ min and $F_{H2O} = 4.5$ g/h.

TABLE IV
RESULTS FOR THE SAMPLES NO. A12 AND THE TWO OPTIMIZED O1 AND O2

№	T_{crys} (°C)	p_{O2} (mbar)	p_{tot} (mbar)	τ_{crys} (min)	F_{N2} (L/min)	p_{H2O} (mbar)	$T_{c,n.}$ (K)	$A_{rc,n.}$ (-)	$J_{c,77K}^{sf}$ (MA/cm²)
A12	770	0.3	250	45	4	3.8	88.5	118	0.15
O1	770	0.2	250	75	3	7.6	87.6	106	0.18
O2	770	0.3	250	75	3	7.6	89.0	50	0.35

TABLE V
ADAPTED PROCESSING WINDOWS FOR THE SECOND DSD (B) RUN

Level (coded units)	X_1 T_{crys} (°C)	X_2 p_{O2} (mbar)	X_3 p_{tot} (mbar)	X_4 τ_{crys} (min)	X_5 F_{H2O} (g/h)
Min (-1)	760	0.15	100	45	2
Center (0)	780	0.225	200	60	4
Max (1)	800	0.3	200	75	6

TABLE VI
BEST RESULTS FOR INDUCTIVE J_c^{sf} (77 K) OF THE SECOND DSD (B) RUN

№	T_{crys} (°C)	p_{O2} (mbar)	p_{tot} (mbar)	τ_{crys} (min)	F_{N2} (L/min)	p_{H2O} (mbar)	$T_{c,n.}$ (K)	$A_{rc,n.}$ (-)	$J_{c,77K}^{sf}$ (MA/cm²)
B12	760	0.3	300	60	3	4.1	89.8	291	1.3

While there was no residual plot with high accuracy possible for $A_{rc,norm}$ ($R^2 < 0.7$), its only significant factor was T_{crys} and also predicting the lower level (−1) of 770 °C (s. Fig. 3) to be optimum. Therefore, further optimization with the above values was done.

C. Optimization

Based on the suggested values for the parameters and for a more profound investigation of the second order effect of p_{O2}, two optimized samples O1 with 0.2 mbar and O2 with 0.3 mbar for p_{O2} were tested (Table IV).

They have a slightly higher/lower value of $T_{c,norm}$ and a similar/half the value of $A_{rc,norm}$ compared to sample No. A12, respectively. Their values and $J_{c,ind}^{sf}$(77 K) are listed in Table IV and for a better assessment with the calculated water p_{H2O} instead of the flow.

With these results, a second DSD (B) run (thickness 590 nm ± 30 nm) was performed with adapted parameter windows (Table V). Due to the significant difference between the two center runs in the first DSD (A), six extra runs were used this time of only one additional center run. Therefore, the total number of samples was 17. This naturally leads to a better data base for the model.

Sample B12 reached 1.3 MA/cm² for $J_{c,ind}^{sf}$(77 K) and also the highest values of $T_{c,norm}$ and $A_{rc,norm}$, the latter confirming better epitaxy (Table VI). This low-pressure of $p_{tot} = 300$ mbar could reduce the carrier gas flow rate by a factor p_{tot}/p_{atm} of 3.3 for equal output as the atmospheric reactor.

XRD only showed slight amounts of residual $BaCeO_3$ and no additional secondary or misoriented phases (Fig. 5).

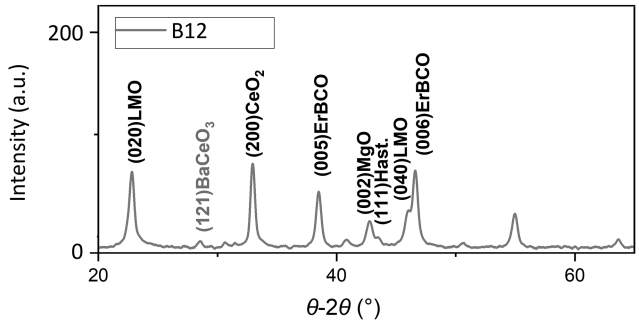

Fig. 5. Theta-2-theta scan of sample B12.

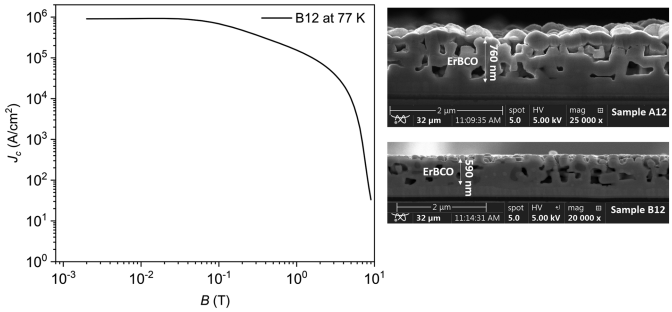

Fig. 6. Resistive $J_c(B, 77\ \mathrm{K})$ of B12 (left) and REM cross section of A12 and B12 (right).

Sample B12 was also tested resistively and in applied magnetic fields. Transport $J_c^{sf}(77\ \mathrm{K})$ was almost 1 MA/cm^2, and the comparison of the cross-section between sample A12 and B12 showed a significantly lower porosity for the latter one, which results in thinner films (Fig. 6). However, the obtained film is still not dense enough to reach high J_c values.

IV. Conclusion

In order to increase the diffusion and thus the film growth rate, the sub-atmospheric crystallization of ErBCO films deposited with CSD on IBAD substrates was optimized via DSD.

This allowed investigating the effects of the crystallization parameters at lower p_{tot} with a greatly reduced number of trials compared to conventional OFAT. Crystallization was optimized regarding resistive $J_c^{sf}(77\ \mathrm{K})$ from nearly zero to 1 MA/cm^2 obtained with $p_{tot} = 300$ mbar, $T_{crys} = 760$ °C, $p_{O2} = 0.3$ mbar, and $p_{H2O} = 4.1$ mbar. Further characterizations confirmed lower porosity by SEM and better epitaxy by rocking curve measurements. This shows that DSD is a very attractive approach to optimize the properties of CSD-grown films, especially for long coated conductors to enhance the growth rate or possibly achieve a reduction of carrier gas flow rate by a factor p_{tot}/p_{atm} of 3.3 for equal output in a reel-to-reel process as the atmospheric reactor. The DSD approach can be moved forward to lower the residual porosity of the obtained films, because this is still the main parameter limiting percolating currents.

References

[1] V. Solovyov, I. K. Dimitrov, and Q. Li, "Growth of thick $YBa_2Cu_3O_7$ layers via a barium fluoride process," *Supercond. Sci. Technol.*, vol. 26, no. 1, 2013, Art. no. 13001.

[2] H. Chen, K. Zalamova, A. Pomar, X. Granados, T. Puig, and X. Obradors, "Nucleation and growth rate influence on microstructure and critical currents of TFA-$YBa_2Cu_3O_7$ under low-pressure conditions," *J. Mater. Res.*, vol. 25, no. 12, pp. 2371–2379, 2010.

[3] I. Yamaguchi et al., "Metal organic deposition of epitaxial Y123 films using a low-cost vacuum technique," *IEEE Trans. Appl. Supercond.*, vol. 15, no. 2, pp. 2927–2930, Jun. 2005.

[4] A. Queraltó et al., "Combinatorial screening of cuprate superconductors by drop-on-demand inkjet printing," *J. Mater, Chem.*, vol. 13, pp. 9101–9112, 2022.

[5] M. Erbe et al., "Comparative study of CSD-grown *RE*BCO films with different rare earth elements: Processing windows and T_c," *Supercond. Sci. Technol.*, vol. 33, no. 9, 2020, Art. no. 94002.

[6] J. Bradley and C. J. Nachtsheim, "A class of three-level designs for definitive screening in the presence of second-order effects," *J. Qual. Technol.*, vol. 43, no. 1, pp. 1–15, 2011.

[7] R. Hayasaka et al., "Investigation of the crystallization process of CSD-ErBCO on IBAD-substrate via DSD approach," *Sci. Rep.*, vol. 10, no. 1, 2020, Art. no. 19934.

[8] H. Rijckaert et al., "Unravelling the crystallization process in solution-derived $YBa_2Cu_3O_{7-\delta}$ nanocomposite films with preformed ZrO_2 nanocrystals via definitive screening design," *J. Phys. Chem. Lett.*, vol. 12, pp. 2118–2125, 2021.

[9] K. P. Burnham and D. R. Anderson, "Multimodel inference," *Sociol. Methods Res.*, vol. 33, no. 2, pp. 261–304, 2004.

[10] D. C. Montgomery, *Design and Analysis of Experiments*, 8th ed., Hoboken, NJ, USA: Wiley, 2019, p. 285ff.

[11] M. H. Kutner, C. J. Nachtsheim, J. Neter, and W. Li, *Appl. Linear Stat. Models*, 5th ed., New York, NY, USA: McGraw-Hill Irwin, 2005, p. 47ff.